HHS Public Access

Author manuscript

Cell Rep. Author manuscript; available in PMC 2024 February 16.

Published in final edited form as:

Cell Rep. 2023 October 31; 42(10): 113161. doi:10.1016/j.celrep.2023.113161.

Post-synaptic $GABA_A$ receptors potentiate transmission by recruiting CaV2 channels to their inputs

Jian Zhao[1,2], **Luna Gao**[1,2], **Stephen Nurrish**[1,2], **Joshua M. Kaplan**[1,2,3,4,*]

[1]Department of Molecular Biology, Massachusetts General Hospital, Boston, MA 02114, USA

[2]Department of Neurobiology, Harvard Medical School, Boston, MA 02115, USA

[3]Program in Neuroscience, Harvard Medical School, Boston, MA 02115, USA

[4]Lead contact

SUMMARY

We describe a retrograde synaptic signal at the *C. elegans* GABAergic neuromuscular junction. At this synapse, GABA release is controlled by two voltage-activated calcium channels (UNC-2/CaV2 and EGL-19/CaV1), and muscle responses are mediated by a single GABA receptor (UNC-49/$GABA_A$). Mutations inactivating UNC-49 or those preventing UNC-49 synaptic clustering cause retrograde defects in GABAergic motor neurons, whereby UNC-2/CaV2 levels at active zones, UNC-2 current, and pre-synaptic GABA release are decreased. Inactivating post-synaptic $GABA_A$ receptors has no effect on GABA neuron EGL-19/CaV1 levels nor on several other pre-synaptic markers. The effect of $GABA_A$ receptors on pre-synaptic strength is not a consequence of decreased GABA transmission and is input selective. Finally, pre-synaptic UNC-2/CaV2 levels are increased when post-synaptic $GABA_A$ receptors are increased but are unaffected by increased extra-synaptic receptors. Collectively, these results suggest that clustered post-synaptic $GABA_A$ receptors adjust the strength of their inputs by recruiting CaV2 to contacting active zones.

In brief

Retrograde synaptic signals allow postsynaptic cells to adjust the strength and plasticity of their synaptic inputs. Zhao et al. show that clustered post-synaptic $GABA_A$ receptors stimulate release by recruiting calcium channels to contacting active zones.

Graphical Abstract

*Correspondence: kaplan@molbio.mgh.harvard.edu.

AUTHOR CONTRIBUTIONS

J.Z. performed electrophysiological analysis of motor neurons and muscles, quantified CaV channel and AZ protein synaptic fluorescence, and constructed strains. L.G. analyzed muscle CaV currents. S.N. designed and isolated CRISPR alleles and constructed strains. J.M.K. supervised and acquired funding. J.M.K., J.Z., L.G., and S.N. wrote and revised the paper.

DECLARATION OF INTERESTS

The authors declare no competing interests.

SUPPLEMENTAL INFORMATION

Supplemental information can be found online at https://doi.org/10.1016/j.celrep.2023.113161.

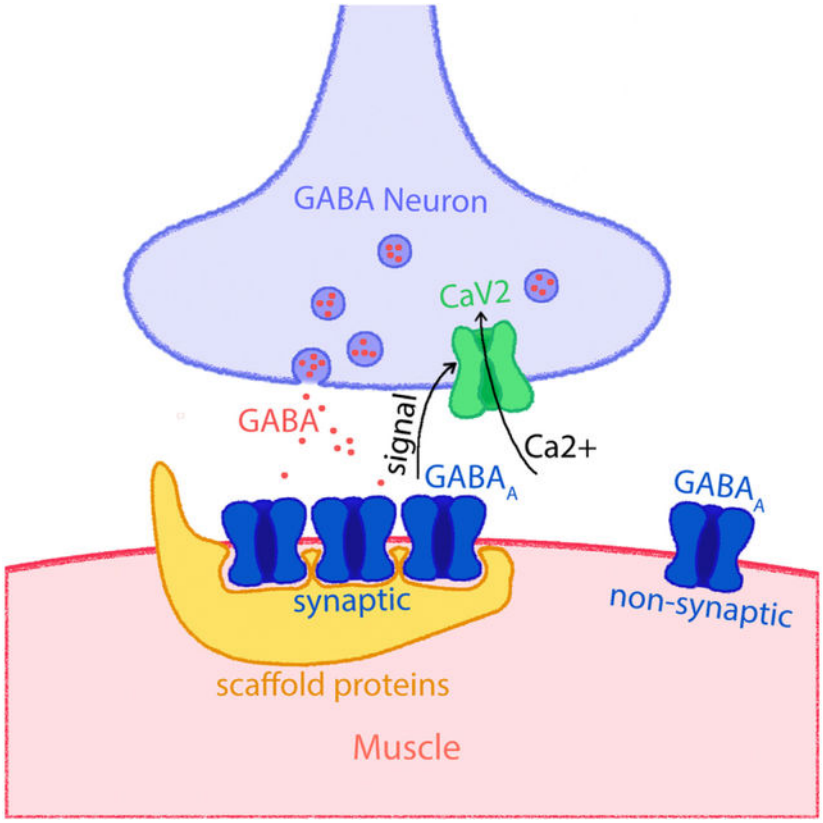

INTRODUCTION

Post-synaptic cells adjust the strength of their synaptic inputs via multiple mechanisms, which are generically designated retrograde synaptic signals. Changes in target cell activity can elicit release of retrograde signals that alter pre-synaptic activity.[1] These activity-dependent retrograde signals include growth factors (e.g., BMP or BDNF), gases (e.g., nitric oxide), conventional neurotransmitters, and lipid-derived signals (e.g., endocannabinoids). Activity-dependent retrograde signals mediate feedback regulation and homeostatic synaptic plasticity.[2,3] Pre-synaptic homeostatic plasticity (PHP) provides a mechanism to stabilize circuit activity during developmental growth and in the face of fluctuating synaptic signals. The mechanisms mediating PHP are broadly conserved in both vertebrates and invertebrates.[4–8] Consequently, PHP is generally considered a ubiquitous form of synaptic plasticity.

Beyond activity-dependent retrograde signals, target cells can stably alter the strength and short-term plasticity of their synaptic inputs.[9] For example, synapses on a single axon can have widely divergent release probabilities depending on the target cell identity.[10–12] These target-derived signals expand the coding capacity of microcircuits by allowing neurons to convey different aspects of their activity to different downstream targets.[13] A few molecules have been identified that mediate these target-derived signals, including elfn1 and its pre-synaptic binding partner mGluR7[14,15]; however, the precise mechanism by which elfn1 and mGluR7 alter release probability has not been defined.[16]

Recent studies suggest that pre-synaptic release sites and post-synaptic densities (PSDs) are aligned across synapses in nanocolumns.[17,18] Transsynaptic alignment is proposed to decrease the delay of post-synaptic responses, to increase the efficiency of post-synaptic receptor activation following synaptic vesicle (SV) fusion, and to mediate retrograde regulation of presynaptic release probability.[17,18] These effects are thought to be mediated by transsynaptic tethering of active zone (AZ) proteins to post-synaptic receptor complexes.[19–21] Several papers show that AZ molecules (e.g., neurexin and a2d2) immobilize receptors in PSDs.[22–25] Thus far, it remains unclear if post-synaptic proteins recruit critical pre-synaptic components to AZs. Here we show that post-synaptic $GABA_A$ receptors function as a target-derived signal that boosts release probability by recruiting voltage-gated calcium (CaV) channels to AZs.

RESULTS

Mutations inactivating UNC-49/$GABA_A$ receptors decrease UNC-2/CaV2 abundance at active zones

C. elegans body muscles receive direct inhibitory input from GABAergic motor neurons.[26] At this synapse, GABA release is controlled by two CaV channels, UNC-2/CaV2 and EGL-19/CaV1,[27] while muscle responses are mediated by a single GABA receptor, UNC-49/$GABA_A$.[28] Endogenous UNC-2/CaV2 and EGL-19/CaV1 channels were labeled with split GFP. Using CRISPR, we introduced the eleventh β strand of GFP (GFP_{11}) into the endogenous *unc-2* and *egl-19* genes. The rate of miniature excitatory post-synaptic currents (mEPSCs) recorded from body muscles is significantly decreased in *unc-2* null mutants[19] but was unaffected in *unc-2*(*nu586* GFP_{11}) mutants (Figures S1A and S1B). Similarly, CaV currents recorded from body muscles are completely blocked by nemadipine (an EGL-19 antagonist)[29,30] but were unaffected in *egl-19*(*nu674* GFP_{11}) mutants (Figures S1C and S1D). These results suggest that the GFP_{11} tag did not significantly impair UNC-2/CaV2 or EGL-19/CaV1 function. Using these tagged alleles, we visualized UNC-2 and EGL-19 expression by expressing $GFP_{1–10}$ in GABA neurons. Pre-synaptic regions were identified using an SV-associated protein, UNC-57/endophilin tagged with mCherry. As expected, both CaV channels exhibited punctate fluorescence in axons (Figures 1A and 1C). The UNC-2/CaV2 signal exhibited a more pronounced enrichment at pre-synapses (Figure 1A), while EGL-19/CaV1 puncta were less tightly associated with the UNC-57/endophilin signal (Figure 1C). Similar UNC-2 and EGL-19 distributions at pre-synaptic terminals were recently described.[31]

Next, we asked if mutants lacking UNC-49/$GABA_A$ have altered CaV abundance in GABA neurons. Consistent with this idea, UNC-2/CaV2 puncta intensity was significantly reduced at GABA neuron pre-synaptic regions in *unc-49*/$GABA_A$ mutants (Figures 1A and 1B), whereas pre-synaptic EGL-19/CaV1 puncta intensity was unaltered (Figures 1C and 1D). The decreased UNC-2/CaV2 puncta intensity in *unc-49* mutants was rescued by a single-copy transgene expressing the UNC-49B isoform in body muscles (Figures 1A and 1B), confirming that muscle $GABA_A$ receptors alter pre-synaptic UNC-2/CaV2 levels in GABA motor neurons.

To determine if the molecular composition of pre-synapses was broadly disrupted in *unc-49*/$GABA_A$ mutants, we analyzed several other AZ proteins. The pre-synaptic levels of UNC-10/RIM, SYD-2/liprin-α, RAB-3, and NRX-1/neurexin-α were analyzed using CRISPR alleles carrying fluorescent tags in the corresponding endogenous genes. These proteins are labeled at all synapses; consequently, we quantified their puncta fluorescence at GABA neuron pre-synapses, which were identified by expressing mCherry-tagged UNC-57/endophilin in GABA neurons. Using this strategy, we found that UNC-10/RIM, SYD-2/liprin-α, RAB-3, and NRX-1/neurexin-α levels at GABA pre-synapses were unaltered in *unc-49*/$GABA_A$ mutants (Figures 1E and 1F). A potential limitation of this analysis is that expression at other synapses could confound analysis of GABA synapses. To address this concern, we repeated the UNC-2 analysis using a CRISPR allele tagged with mNeonGreen, *unc-2*(*nu657* mNG). As seen with *unc-2*(*nu586* GFP_{11}), *unc-2*(*nu657* mNG) puncta intensity at GABA pre-synapses was significantly decreased in *unc-49* mutants (Figures S1E and S1F). Collectively, these results suggest that muscle $GABA_A$ receptors selectively adjust pre-synaptic UNC-2/CaV2 levels while having little impact on several other pre-synaptic proteins. Our analysis is restricted to pre-synaptic regions (labeled by UNC-57/mCherry); consequently, it remains possible that protein levels in extra-synaptic regions are altered in *unc-49* mutants.

UNC-2/CaV2 currents are decreased in *unc-49*/$GABA_A$ mutants

To assess UNC-2/CaV2 channel function, we recorded CaV currents (I_{Cav}) in GABA neurons. *C. elegans* lacks voltage-activated sodium channels[32]; consequently, voltage-activated currents comprise a mixture of calcium and potassium currents. We isolated the calcium currents by adding potassium channel blockers to the recording solutions. Using these conditions, we detected small voltage-activated inward currents in wild-type GABA neurons (Figure 2A). Several results suggest that these are calcium currents. The voltage-dependence of this current is similar to those expected for CaV channels, with peak currents observed at 0–10 mV (Figure 2B). These currents reversed at ~+50 mV, which corresponds to the predicted calcium equilibrium potential (Figure 2B). Finally, these currents were blocked by a general CaV antagonist (Cd^{2+}), confirming that they were calcium currents (Figures 2A and 2B). Addition of a potent EGL-19/CaV1 antagonist (nemadipine) eliminated about half of the I_{CaV} current (Figures 2A and 2B). Similarly, the I_{CaV} current recorded from *unc-2*/CaV2 mutant neurons was about half that observed in wild-type (WT) controls (Figures 2A and 2B). This residual I_{CaV} current was eliminated in recordings from nemadipine-treated *unc-2*/CaV2 mutant neurons (Figures 2A and 2B). Thus, EGL-19/CaV1 and UNC-2/CaV2 channels contribute equally to I_{CaV} currents in GABA motor neurons. Hereafter, we refer to I_{Cav} recorded in the presence of nemadipine as the UNC-2/CaV2 current. The EGL-19 current (recorded in *unc-2* mutants) and UNC-2 current reversed at slightly different membrane potentials (Figure 2B), most likely due to subtle differences in the ion selectivity of these channels.

Next, we analyzed *unc-49*/$GABA_A$ mutants and found that the I_{CaV} current recorded from GABA neurons was significantly reduced (Figures 2C–2F). The impact of *unc-49* mutations on I_{CaV} was unaffected by nemadipine (Figures 2E and 2F), suggesting that the UNC-49-sensitive I_{CaV} current was not mediated by EGL-19/CaV1 channels. By contrast,

the impact of *unc-49* mutations on I_{CaV} was eliminated in *unc-49*; *unc-2* double mutants (Figures 2C and 2D), indicating that the UNC-49-sensitive I_{CaV} current was mediated by UNC-2/CaV2 channels. I_{CaV} activation kinetics were unaltered in *unc-49*/$GABA_A$ mutants, suggesting that the remaining UNC-2 and EGL-19 channels functioned normally (Figures 2E and 2G). The decreased UNC-2/CaV2 current in *unc-49*/$GABA_A$ mutants was rescued by a single-copy transgene expressing the UNC-49B isoform in body muscles (Figures 2C and 2D). Taken together, these results suggest that mutations inactivating muscle UNC-49/$GABA_A$ receptors decreased UNC-2/CaV2 current in GABA neurons (32% decrease, Figure 2D), which mirrors the decreased UNC-2 puncta intensity observed in these mutants (32% decrease, Figure 1B). The identical changes in UNC-2 fluorescence and current observed in *unc-49* mutants suggests that nearly all neuronal UNC-2 resides on the cell surface at AZs. Lack of an intracellular UNC-2 pool at synapses is consistent with the failure to detect an internal CaV2 pool at mammalian synapses by immunoelectron microscopy.[33,34]

Next, we asked if other ion channels in GABA motor neurons are disrupted in *unc-49*/$GABA_A$ mutants. To address this question, we analyzed voltage-activated potassium currents (I_K), resting membrane potential (RMP), and input resistance (R_{in}, a measure of leak currents). We found that GABA neuron I_K, RMP, and R_{in} were unaffected in *unc-49* mutants (Figure S2). These results suggest that the absence of UNC-49/$GABA_A$ receptors did not broadly alter motor neuron ion channels and excitability.

Blocking GABA release has no effect on UNC-2/CaV2 levels in motor neurons

The decreased UNC-2/CaV2 levels observed in *unc-49*/$GABA_A$ mutants could represent a compensatory response triggered by decreased GABA transmission. This seems unlikely because the effect we observe (decreased UNC-2/CaV2) would exacerbate the GABA transmission defect rather than mitigate it. Nonetheless, it remains possible that the UNC-2/CaV2 defect is a secondary consequence of decreased GABA transmission. To address this possibility, we analyzed UNC-2 levels in GABA neurons following blockade of GABA release. A mutation inactivating the vesicular GABA transporter (UNC-47/VGAT) dramatically decreased muscle mIPSC amplitude and rate (Figures 3A–3C), both indicating reduced GABA release. By contrast, the *unc-47*/VGAT mutation had no effect on UNC-2/CaV2 puncta intensity nor on UNC-2/CaV2 current (Figures 3D–3G). These results suggest that decreased GABA transmission is unlikely to account for the decreased GABA neuron UNC-2/CaV2 levels observed in *unc-49*/$GABA_A$ mutants.

UNC-49/$GABA_A$ effects on UNC-2/CaV2 are input specific

Decreased UNC-2/CaV2 levels in GABA neurons could reflect circuit-wide changes triggered by inactivating muscle $GABA_A$ receptors. To address this possibility, we analyzed UNC-2/CaV2 levels in cholinergic (ACh) motor neurons. We found that ACh neuron UNC-2/CaV2 puncta intensities and UNC-2 currents were not significantly altered in *unc-49*/$GABA_A$ mutants (Figures 4A–4D). These results suggest that muscle UNC-49/$GABA_A$ receptors selectively regulate the strength of GABA motor neuron inputs without impacting excitatory input from cholinergic motor neurons.

UNC-49's impact on UNC-2/CaV2 is mediated by clustered synaptic receptors

UNC-49/$GABA_A$ receptors on the surface of muscles comprise two pools, diffuse extra-synaptic receptors and clustered receptors localized at post-synapses. To determine which pool controls GABA neuron UNC-2/CaV2 levels, we analyzed mutants lacking scaffolding proteins (LIN-2/CASK, FRM-3/FARP, and NLG-1/neuroligin) that immobilize UNC-49 receptors at post-synapses.[35–38] In *lin-2* mutants, total surface and synaptic UNC-49/$GABA_A$ levels are both reduced.[39] By contrast, in *frm-3* and *nlg-1* mutants, total surface UNC-49/$GABA_A$ levels are unaltered, whereas clustered synaptic receptors are dramatically reduced.[35,39] Thus, these mutants allow us to determine if synaptic or extra-synaptic receptors mediate UNC-49's impact on UNC-2/CaV2 levels in GABA neurons.

The intensity of UNC-2/CaV2 synaptic puncta in GABA neurons was significantly reduced in mutants lacking any of these scaffolding proteins (Figures 5A and 5B). Similar decreases in GABA neuron UNC-2/CaV2 currents were also observed in these scaffolding mutants (Figures 5C and 5D). The impact of FRM-3/FARP on motor neuron UNC-2/CaV2 levels and current was eliminated in *frm-3; unc-49* double mutants (Figures 5A–5D), consistent with FRM-3 controlling neuronal UNC-2 levels via changes in muscle UNC-49 receptors. Changes in neuronal UNC-2/CaV2 levels could result from the absence of scaffolding proteins from neurons or muscles. To distinguish between these possibilities, we used CRISPR to construct an allele that is inactivated by CRE recombinase, *frm-3(nu751)*/FARP. Using this allele, we found that muscle-specific *frm-3* knockouts significantly reduced UNC-2/CaV2 puncta intensity and current in GABA neurons, whereas neuron-specific knockouts had no effect (Figures S3A–S3D). Thus, these results strongly support the idea that UNC-2/CaV2 levels in GABA neurons are controlled by clustered UNC-49/$GABA_A$ receptors immobilized at postsynaptic elements.

GABA release is decreased in *frm-3*/FARP mutants

If pre-synaptic UNC-2/CaV2 levels are decreased in post-synaptic scaffolding mutants, we would expect that GABA release would be reduced. We did several experiments to test this idea. First, we measured the rate of miniature inhibitory postsynaptic currents (mIPSCs), which is often used as a measure of GABA release. The mIPSC rate was significantly reduced in both *nlg-1* and *lin-2* mutants (Figures 6A and 6B). Several results suggest that this decreased mIPSC rate is unlikely to result from decreased GABA release. First, mIPSC rates and amplitudes were unaffected in *unc-2* CaV2 null mutants (Figures 6A–6C), as previously reported.[27] The mIPSC rates in *unc-2* mutants are unaltered because UNC-2/CaV2 and EGL-19/CaV1 act redundantly to promote spontaneous GABA release at this synapse.[27] Second, unlike *nlg-1* and *lin-2* mutants, mIPSC rates were unaffected in *frm-3* mutants (Figures 6A and 6B), despite the fact that frm-3 mutants also have decreased pre-synaptic UNC-2 levels (Figure 5).

An alternative explanation for decreased mIPSC rates is that smaller mIPSC amplitudes in scaffold mutants decrease mIPSC detection. In *frm-3, nlg-1*, and *lin-2* mutants, mIPSC amplitudes were significantly reduced (Figures 6A, 6C, and S4A), as a consequence of decreased UNC-49/$GABA_A$ post-synaptic localization.[35–37,39] The mIPSC amplitudes in *frm-3* mutants comprise a multiplicatively scaled version of the WT distribution, consistent

with a uniform 39% decrease in amplitude (Figure S4B). By contrast, mIPSC amplitudes in *lin-2* and *nlg-1* mutants were not multiplicatively scaled versions of the WT distribution (Figures S4C and S4D), due to the apparent loss of smaller mIPSCs. Taken together, these results suggest that decreased mIPSC rates in *lin-2* and *nlg-1* mutants result from decreased detection of small mIPSCs. By contrast, the normal mIPSC rate in *frm-3* mutants suggests that mIPSCs are accurately detected, most likely due to a more modest decrease in mIPSC amplitudes compared to *lin-2* and *nlg-1* mutants (Figure S4A).[39]

As an alternative measure of GABA release, we next analyzed quantal content (the total number of SVs released during an evoked response). Quantal content (QC) is calculated as the ratio of the stimulus-evoked inhibitory post-synaptic current (IPSC) amplitude to the mean mIPSC amplitude in the same cell. Thus, assaying QC requires that mIPSC amplitudes are accurately measured. The preceding results suggest that mIPSCs are accurately detected in *frm-3* mutants; consequently, we utilized this strain to analyze QC. We found that the evoked IPSC amplitude and the QC of evoked responses were both significantly reduced in *frm-3* mutants (Figures 6D–6F). These results suggest that presynaptic GABA release was decreased in *frm-3* mutants, consistent with the decreased GABA neuron UNC-2/CaV2 levels found in these mutants (Figure 5). The QC observed in *unc-2* null mutants was smaller than that in *frm-3* mutants (Figure 6F), consistent with the incomplete loss of GABA neuron UNC-2 in *frm-3* mutants observed by both imaging and calcium current recordings (Figure 5).

Increasing muscle UNC-49/GABAA levels increases UNC-2/CaV2 levels in GABA motor neurons

Thus far, our results suggest that decreasing post-synaptic UNC-49/$GABA_A$ levels produces a corresponding decrease in UNC-2/CaV2 levels in GABA motor neurons. If $GABA_A$ receptors are an instructive signal that actively recruits UNC-2/CaV2 to contacting AZs, we would expect that the converse effect would be observed when muscle UNC-49 levels are increased. To test this idea, we constructed two transgenes that over-express UNC-49 in body muscles. The first transgene (hereafter UNC-49XS) over-expresses the UNC-49B isoform. A second transgene (hereafter synUNC-49XS) jointly over-expresses UNC-49B together with its scaffolds (FRM-3/FARP, LIN-2/CASK, and NLG-1). As previously reported,[35] the UNC-49XS transgene greatly increased the GABA-activated current recorded from muscles (Figures S5A and S5B) but had no effect on either mIPSC rates or amplitudes (Figures S5C and S5E), suggesting that UNC-49XS increases extra-synaptic UNC-49 receptors while having no effect on synaptic UNC-49 levels. By contrast, the synUNC-49XS transgene increased the GABA-activated current (Figures S5A and S5B), as well as the frequency and amplitudes of muscle mIPSCs (Figures S5C–S5E), suggesting that this transgene increased the levels of both synaptic and extra-synaptic UNC-49 receptors.

Next, we asked if GABA neuron UNC-2/CaV2 levels are altered by increased muscle UNC-49/$GABA_A$ levels (Figure 7). UNC-2/CaV2 puncta intensity and current were not significantly altered in UNC-49XS animals (Figures 7A–7D), suggesting that increased extra-synaptic UNC-49/$GABA_A$ levels had no effect on pre-synaptic UNC-2/CaV2

channels. By contrast, UNC-2/CaV2 puncta intensity and current were significantly increased in synUNC-49XS animals (Figures 7A–7D), suggesting that increasing the levels of synaptic UNC-49/$GABA_A$ receptors was sufficient to elicit corresponding increases in pre-synaptic UNC-2/CaV2. By contrast, GABA neuron potassium currents, RMP, and input resistance were unaltered in synUNC-49XS animals, suggesting that other ion channels were unaffected (Figure S6). Collectively, these results suggest that post-synaptic $GABA_A$ receptors bidirectionally adjust pre-synaptic UNC-2/CaV2 levels in the AZs of GABA motor neurons.

DISCUSSION

Our results lead to four principal conclusions. First, muscle UNC-49/$GABA_A$ receptors promote GABA release at neuromuscular junctions (NMJs). Second, muscle $GABA_A$ receptors regulate release probability by recruiting UNC-2/CaV2 channels to AZs. Third, clustered post-synaptic UNC-49/$GABA_A$ receptors control pre-synaptic UNC-2/CaV2 levels, whereas extra-synaptic UNC-49 receptors have no effect. Fourth, the *C. elegans* GABAergic NMJ does not exhibit PHP, suggesting that PHP is not conserved at all synapses. Below we discuss the significance of these findings.

UNC-49/$GABA_A$ receptors are a target-derived signal that boosts pre-synaptic release

Several prior studies showed that target cell identity adjusts the strength and short-term plasticity of synaptic inputs. These effects have been seen in rodents, in insects, at central synapses, and at NMJs. Only a few molecules have previously been identified as target-derived signals, most notably elfn1.[14]

Here we identify post-synaptic $GABA_A$ receptors as a target-derived signal that enhances pre-synaptic strength by recruiting CaV2 channels to contacting AZs. Several results suggest that muscle $GABA_A$ receptors have a relatively direct effect on AZ UNC-2/CaV2 levels in GABA neurons. Many other GABA neuron AZ markers and ion channels were unaffected in *unc-49*/$GABA_A$ mutants. Blocking pre-synaptic GABA release had no effect on pre-synaptic CaV2, suggesting that this effect was not a secondary consequence of decreased GABAergic transmission. This effect was mediated by synaptic $GABA_A$ receptors, whereas extra-synaptic receptors had no effect on pre-synaptic UNC-2/CaV2 levels. This effect was input specific, i.e., muscle $GABA_A$ receptors adjust CaV2 levels in the AZs of GABA neurons but not those in ACh motor neurons. This effect was bidirectional; i.e., increased and decreased synaptic $GABA_A$ receptors elicited corresponding changes in pre-synaptic CaV2. Collectively, these results are most consistent with $GABA_A$ post-synaptic clusters directly adjusting CaV2 levels in their pre-synaptic inputs.

Interestingly, we found that eliminating pre-synaptic UNC-2/CaV2 channels (i.e., in *unc-2* null mutants) had no effect on mIPSC amplitude, consistent with a prior study.[27] Post-synaptic UNC-49/$GABA_A$ levels strongly correlate with mIPSC amplitudes[35–38]; consequently, these results suggest that post-synaptic UNC-49/$GABA_A$ levels were not significantly decreased in *unc-2*/CaV2 mutants. Thus, the regulatory interaction between pre-synaptic UNC-2/CaV2 and post-synaptic UNC-49 appears to be asymmetric, with

altered muscle UNC-49 levels producing corresponding changes in neuronal UNC-2 but not vice versa.

By contrast, a prior study showed that increased expression of a CaV auxiliary subunit (CACNA2D2) triggers an increase in postsynaptic $GABA_A$ receptors.[40] Interestingly, CACNA2D2 had this effect even when expressed in glutamatergic neurons, providing support for the idea that CACNA2D2 could be physically coupled across the synapse to $GABA_A$ receptor clusters. These results (together with our findings) support the idea that CaV2 and $GABA_A$ channels are linked transsynaptically and that this linking provides a cell biological mechanism to produce correlated changes in pre- and post-synaptic strength.

Could this represent a general mechanism? Several results support this idea. At both glutamatergic and GABAergic synapses, pre-synaptic release sites are aligned with post-synaptic receptors in nanocolumns,[17,41] consistent with their transsynaptic linkage. CACNA2D subunits have been shown to recruit postsynaptic receptors at a variety of synapses,[25,40,42] also consistent with transsynaptic linking of CaV channels with neurotransmitter receptors. Finally, in cultured hippocampal neurons, post-synaptic glutamate receptors were previously proposed to boost release; however, in this case, the effect was mediated by an enlarged pool of releasable SVs without altering release probability.[43] Collectively, these results suggest that post-synaptic receptors could function as target-derived signals regulating pre-synaptic release at many synapses. Post-synaptic receptors likely co-assemble with different binding partners (e.g., scaffolds, synaptic cell adhesion molecules, transmembrane proteins, and extracellular matrix proteins) at different synapses; consequently, the structural diversity of synaptic receptor complexes could produce a correspondingly diverse set of target-derived signals.

Implications for understanding synaptic plasticity

At many synapses (including rodent central synapses and both fly and rodent NMJs), disrupting post-synaptic receptors triggers compensatory responses (termed pre-synaptic homeostatic plasticity, PHP).[4–8,44] PHP restores synaptic function by boosting neurotransmitter release through a variety of mechanisms, including increased calcium entry through pre-synaptic CaV channels.[2,45] Thus, PHP promotes pre-synaptic release in response to decreased synaptic strength, opposite to the effect we observed at the worm GABAergic NMJ. In *C. elegans*, disrupting post-synaptic $GABA_A$ receptors elicits retrograde inhibition, whereby pre-synaptic CaV2 abundance, CaV2 current, and GABA release are diminished. This effect was observed in both $GABA_A$ null mutants and in scaffold mutants (where post-synaptic currents are diminished but not eliminated). Thus, our results suggest that the *C. elegans* GABAergic NMJ does not exhibit an effective form of PHP. These results show that PHP is not ubiquitous and that only certain animals evolved the ability to perform homeostatic adjustments of pre-synaptic function to stabilize synaptic transmission. Given the detailed knowledge of the genetic mechanisms involved in PHP,[2,45] it will be interesting to determine if *C. elegans* lacks a specific essential PHP signaling component.

Some Hebbian forms of synaptic plasticity, e.g., long-term potentiation (LTP) and depression (LTD), are mediated by activity-induced changes in post-synaptic receptor

abundance. If the mechanism described here is conserved at mammalian synapses, this would suggest that changes in post-synaptic glutamate receptors (following LTP or LTD) might subsequently elicit corresponding changes in pre-synaptic CaV2 levels. This could potentially explain why LTP is often associated with a subsequent balanced increase in the size and function of pre- and post-synaptic elements.[46] Similarly, ultrastructural studies suggest that there is a transsynaptic matching of pre- and post-synaptic sizes across many brain regions.[47,48] It will be interesting to determine if the matching of pre- and post-synaptic sizes and strengths is mediated by linking pre-synaptic CaV channels with post-synaptic receptor clusters.

Limitations of the study

This study has several notable limitations. First, all data were derived from analysis of genetic mutants in intact worms; consequently, indirect effects of mutations altering $GABA_A$ receptors may contribute to our results. Second, we describe this effect at a single synapse, the GABAergic NMJ. It will be important to determine if post-synaptic receptors have similar effects at other synapses. Third, in many animals, changes in post-synaptic strength elicit compensatory homeostatic responses (i.e., PHP). In these cases, PHP would obscure the retrograde inhibitory effects described here. Thus, it will be important to determine how these two mechanisms interact in other organisms.

STAR★METHODS

RESOURCE AVAILABILITY

Lead contact—Further information and requests for resources and reagents should be directed to and will be fulfilled by the lead contact, Joshua M. Kaplan (kaplan@molbio.mgh.harvard.edu).

Materials availability—All unique reagents generated in this study are available from the lead contact with a completed materials transfer agreement.

Data and code availability

- Data reported are available upon request from the lead contact.
- This paper does not report original code.
- Any additional information required to reanalyze the data reported in this paper is available from the lead contact upon request.

EXPERIMENTAL MODEL AND SUBJECT DETAILS

Animals—*C. elegans* strains were cultivated at room temperature (~22°C) on agar nematode growth media seeded with OP50 bacteria. Unless otherwise stated, the wild-type animal refers to the Bristol N2 strain. Alleles and strains used in this study are listed in the key resources table. Transgenic animals were prepared by microinjection, and integrated transgenes were isolated following UV irradiation, as described.[49] Single copy transgenes were isolated by the MoSCI and miniMoS techniques.[50,51]

METHOD DETAILS

CRISPR alleles—CRISPR alleles were isolated as described.[52] Briefly, we used *unc-58* as a co-CRISPR selection to identify edited animals. Animals were injected with two guide RNAs (gRNAs) and two repair templates, one introducing an *unc-58* gain of function mutation and a second modifying a gene of interest. Progeny exhibiting the *unc-58*(gf) uncoordinated phenotype were screened for successful editing of the second locus by PCR. Split GFP constructs are as described.[53] All CRISPR alleles were outcrossed 5 times to eliminate off target mutations. MiniMOS transgenes expressing $GFP_{1–10}$:SL2UNC-57/mCherry in GABA neurons (*nuSi285*, *unc-47* promoter) or ACh neurons (*nuSi250*, *unc-129* promoter) were used to visualize GFP_{11} tagged proteins.

Tissue specific knockouts were performed using CRE inactivated alleles. CRE recombinase was expressed in muscles (*myo-3* promoter) or neurons (*sbt-1* promoter). Tissue specific *frm-3* knockouts were performed by introducing a stop cassette into intron 3 in the ON configuration (i.e., in the opposite orientation of the target gene) using CRISPR, creating the *frm-3*(*nui751*, *flex ON*) allele, as described.[39] The stop cassette is flanked by FLEX sites (which are modified *loxP* sites that mediate CRE induced inversions).[54] In this manner, *frm-3* expression is reduced following CRE expression.

Fluorescence imaging—Worms were immobilized on 10% agarose pads with 3 μL of 0.1 μm diameter polystyrene microspheres (Polysciences 00876–15, 2.5% w/v suspension). The dorsal nerve cord just anterior to the vulva was imaged. Images were taken with a Nikon A1R confocal, using a 60X/1.49 NA oil objective. Image volumes spanning the dorsal nerve cord were collected (20–30 planes/volume, 0.4 μm between planes, and 0.14 mm/pixel). Maximum intensity projections for each volume were auto-thresholded, and puncta were identified as round fluorescent objects (area >0.1 μm^2), using analysis of particles. Mean fluorescent intensity in each punctum was analyzed in the raw images. Pre-synaptic regions of interest (ROIs) were identified by localization of an mCherry tagged synaptic vesicle marker (UNC-57/Endophilin) expressed in either the ACh or GABA motor neurons. Using CRISPR tagged alleles (see key resources table), the intensity of endogenously expressed active zone markers in the UNC-57 ROIs were quantified. All image analysis was done using FIJI.

Electrophysiology—Whole-cell patch-clamp measurements were performed using an Axopatch 200B amplifier with pClamp 10 software (Molecular Devices). The data were sampled at 10 kHz and filtered at 5 kHz. All recordings were performed at room temperature (~19–21°C). Neurons were identified for patching by expression of transcriptional reporters: P*unc-17*:GFP for ACh neurons and P*unc-25*:RFP for GABA neurons.

Neuron CaV recordings—The bath solution contained (in mM): TEA-Cl 140, $CaCl_2$ 5, $MgCl_2$ 1, 4-AP 3, glucose 10, sucrose 5, and HEPES 15 (pH 7.4, 330 mOsm). The pipette solution contained (in mM): CsCl 140, TEA-Cl 10, $MgCl_2$ 5, KOH 20, Tris 5, $CaCl_2$ 0.25, sucrose 36, EGTA 5 and Na_2ATP 5, Na_2GTP 1, HEPES 10 (adjusted to pH 7.2, 320 mOsm with CsOH). For UNC-2 recordings, 10μM nemadipine was added to the bath solution. In some recordings, a general CaV antagonist (0.3 mM $CdCl_2$) was added to the bath to block

calcium currents. The voltage-clamp protocol consisted of −60mV for 50ms, −90mV for 100 ms, and test voltage (from −60mV to +60mV) for 200 ms. Depolarizing steps were initiated immediately after patching (<30 s). When repeated sets of depolarizing steps were done in a single neuron, I_{CaV} currents were stable for the first 3 sets and declined thereafter. To minimize the impact of I_{CaV} run down, only the first set of depolarizing steps were used for our analysis. In figures, we show inward currents evoked at 0 mV, which elicits the peak UNC-2 current. Macroscopic CaV activation time constants were estimated by fitting individual traces (evoked at 0 mV) to an exponential function.

Neuron I_K recordings—The bath solution contained (in mM): NaCl 140, KCl 5, $CaCl_2$ 5, $MgCl_2$ 5, dextrose 11 and HEPES 5 (pH 7.2, 320 mOsm). The pipette solution contained (in mM): Kgluconate 120, KOH 20, Tris 5, $CaCl_2$ 0.25, $MgCl_2$ 4, sucrose 36, EGTA 5 and Na2ATP 4 (pH 7.2, 320 mOsm). The voltage-clamp protocol consisted of −60mV for 50ms, −90mV for 100 ms, and test voltage (from −60mV to +60mV) for 300 ms.

Neuron RMP and input resistance recordings—The bath solution contained (in mM): NaCl 140, KCl 5, $CaCl_2$ 5, $MgCl_2$ 5, dextrose 11 and HEPES 5 (pH 7.2, 320 mOsm). The pipette solution contained (in mM): Kgluconate 120, KOH 20, Tris 5, $CaCl_2$ 0.25, $MgCl_2$ 4, sucrose 36, EGTA 5 and Na2ATP 4 (pH 7.2, 320 mOsm). RMP was measured in current clamp by holding at 0 pA for 20 s. Input resistance was measured in current clamp by measuring the change in membrane potential evoked by injecting −10 pA.

Muscle IPSC recordings—Body muscle IPSCs were recorded as previously described.[35] Dissected adults were superfused in an extracellular solution containing 127 mM NaCl, 5 mM KCl, 26 mM $NaHCO_3$, 1.25 mM NaH_2PO_4, 10 mM glucose, 5mM sucrose, 1 mM $CaCl_2$, and 4 mM $MgCl_2$, bubbled with 5% CO_2, 95% O_2 at 22°C. The pipette solution contained 105 mM CH_3O_3SCs, 10 mM CsCl, 15 mM CsF, 4mM $MgCl_2$, 5mM EGTA, 0.25mM $CaCl_2$, 10mM HEPES, and 5mM Na_2ATP, 1mM Na_2GTP adjusted to pH 7.2 using CsOH. Whole-cell recordings were carried out at 0mV to record mIPSCs, and −60mV to record mEPSCs. Stimulus-evoked IPSCs were obtained by photo-activating GABA motor neurons (expressing ChR2) with a 3 ms light pulse (Lumencor 470 nm LED). For GABA-activated currents, the holding potential was −60 mV and currents were evoked by a ~0.5 s exposure to pressure ejected 100 mM GABA.

QUANTIFICATION AND STATISTICAL ANALYSIS

For normally distributed data, significant differences were assessed with unpaired t tests (for 2 groups) or one way ANOVA with post-hoc Tukey's multiple comparisons test (for >2 groups). For non-normal data, differences were assessed by Mann-Whitney (2 groups) or Kruskal-Wallis test with post-hoc Dunn's multiple comparisons test (>2 groups). Data graphing and statistics were performed in GraphPad Prism 9. No statistical method was used to select sample sizes. Data shown in each figure represent contemporaneous measurements from mutant and control animals over a period of 1–2 weeks. For electrophysiology, data points represent mean values for individual neuron or muscle recordings (which were considered biological replicates). For imaging studies, data points represent mean puncta

fluorescence values in individual animals (which were considered biological replicates). All data obtained in each experiment were analyzed, without any exclusions.

Supplementary Material

Refer to Web version on PubMed Central for supplementary material.

ACKNOWLEDGMENTS

We thank the following for strains, advice, reagents, and comments on the manuscript: *C. elegans* genetics stock center (CGC), Kang Shen, Zhitao Hu, and members of the Kaplan lab. This work was supported by an NIH research grant to J.K. (NS32196). The CGC is funded by the NIH Office of Research Infrastructure Programs (P40 OD010440).

REFERENCES

1. Regehr WG, Carey MR, and Best AR (2009). Activity-dependent regulation of synapses by retrograde messengers. Neuron 63, 154–170. 10.1016/j.neuron.2009.06.021. [PubMed: 19640475]
2. Davis GW, and Müller M (2015). Homeostatic control of presynaptic neurotransmitter release. Annu. Rev. Physiol. 77, 251–270. 10.1146/annurev-physiol-021014-071740. [PubMed: 25386989]
3. Turrigiano GG, and Nelson SB (2004). Homeostatic plasticity in the developing nervous system. Nat. Rev. Neurosci. 5, 97–107. [PubMed: 14735113]
4. Thiagarajan TC, Piedras-Renteria ES, and Tsien RW (2002). Alpha- and betaCaMKII. Inverse regulation by neuronal activity and opposing effects on synaptic strength. Neuron 36, 1103–1114. 10.1016/s0896-6273(02)01049-8. [PubMed: 12495625]
5. Burrone J, O'Byrne M, and Murthy VN (2002). Multiple forms of synaptic plasticity triggered by selective suppression of activity in individual neurons. Nature 420, 414–418. 10.1038/nature01242. [PubMed: 12459783]
6. Wierenga CJ, Walsh MF, and Turrigiano GG (2006). Temporal regulation of the expression locus of homeostatic plasticity. J. Neurophysiol. 96, 2127–2133. 10.1152/jn.00107.2006. [PubMed: 16760351]
7. Delvendahl I, Kita K, and Muller M (2019). Rapid and sustained homeostatic control of presynaptic exocytosis at a central synapse. Proc. Natl. Acad. Sci. USA 116, 23783–23789. 10.1073/pnas.1909675116. [PubMed: 31685637]
8. Petersen SA, Fetter RD, Noordermeer JN, Goodman CS, and DiA-ntonio A (1997). Genetic analysis of glutamate receptors in Drosophila reveals a retrograde signal regulating presynaptic transmitter release. Neuron 19, 1237–1248. 10.1016/s0896-6273(00)80415-8. [PubMed: 9427247]
9. Tóth K, and McBain CJ (2000). Target-specific expression of pre- and postsynaptic mechanisms. J. Physiol. 525 Pt 1, 41–51. 10.1111/j.1469-7793.2000.00041.x. [PubMed: 10811723]
10. Atwood HL (1967). Variation in physiological properties of crustacean motor synapses. Nature 215, 57–58. 10.1038/215057a0. [PubMed: 4293258]
11. Davis GW, and Murphey RK (1993). A role for postsynaptic neurons in determining presynaptic release properties in the cricket CNS: evidence for retrograde control of facilitation. J. Neurosci. 13, 3827–3838. [PubMed: 8366348]
12. Scanziani M, Gähwiler BH, and Charpak S (1998). Target cell-specific modulation of transmitter release at terminals from a single axon. Proc. Natl. Acad. Sci.USA 95, 12004–12009.10.1073/pnas.95.20.12004. [PubMed: 9751780]
13. Abbott LF, and Regehr WG (2004). Synaptic computation. Nature 431, 796–803. 10.1038/nature03010. [PubMed: 15483601]
14. Sylwestrak EL, and Ghosh A (2012). Elfn1 regulates target-specific release probability at CA1-interneuron synapses. Science 338, 536–540. 10.1126/science.1222482. [PubMed: 23042292]
15. Stachniak TJ, Sylwestrak EL, Scheiffele P, Hall BJ, and Ghosh A (2019). Elfn1-Induced Constitutive Activation of mGluR7 Determines Frequency-Dependent Recruitment of

Somatostatin Interneurons. J. Neurosci. 39, 4461–4474. 10.1523/JNEUROSCI.2276-18.2019. [PubMed: 30940718]

16. Éltes T, Kirizs T, Nusser Z, and Holderith N (2017). Target Cell Type-Dependent Differences in Ca(2+) Channel Function Underlie Distinct Release Probabilities at Hippocampal Glutamatergic Terminals. J. Neurosci. 37, 1910–1924. 10.1523/JNEUROSCI.2024-16.2017. [PubMed: 28115484]
17. Tang AH, Chen H, Li TP, Metzbower SR, MacGillavry HD, and Blanpied TA (2016). A trans-synaptic nanocolumn aligns neurotransmitter release to receptors. Nature 536, 210–214. 10.1038/nature19058. [PubMed: 27462810]
18. Biederer T, Kaeser PS, and Blanpied TA (2017). Transcellular Nano-alignment of Synaptic Function. Neuron 96, 680–696. 10.1016/j.neuron.2017.10.006. [PubMed: 29096080]
19. Tong XJ, López-Soto EJ, Li L, Liu H, Nedelcu D, Lipscombe D, Hu Z, and Kaplan JM (2017). Retrograde Synaptic Inhibition Is Mediated by alpha-Neurexin Binding to the alpha2delta Subunits of N-Type Calcium Channels. Neuron 95, 326–340.e5. 10.1016/j.neuron.2017.06.018. [PubMed: 28669545]
20. Haas KT, Compans B, Letellier M, Bartol TM, Grillo-Bosch D, Sejnowski TJ, Sainlos M, Choquet D, Thoumine O, and Hosy E (2018). Pre-post synaptic alignment through neuroligin-1 tunes synaptic transmission efficiency. Elife 7, e31755. 10.7554/eLife.31755. [PubMed: 30044218]
21. Ramsey AM, Tang AH, LeGates TA, Gou XZ, Carbone BE, Thompson SM, Biederer T, and Blanpied TA (2021). Subsynaptic positioning of AMPARs by LRRTM2 controls synaptic strength. Sci. Adv. 7, eabf3126. 10.1126/sciadv.abf3126. [PubMed: 34417170]
22. Nam CI, and Chen L (2005). Postsynaptic assembly induced by neurexin-neuroligin interaction and neurotransmitter. Proc. Natl. Acad. Sci. USA 102, 6137–6142. [PubMed: 15837930]
23. Kang Y, Zhang X, Dobie F, Wu H, and Craig AM (2008). Induction of GABAergic postsynaptic differentiation by alpha-neurexins. J. Biol. Chem. 283, 2323–2334. [PubMed: 18006501]
24. Heine M, Thoumine O, Mondin M, Tessier B, Giannone G, and Choquet D (2008). Activity-independent and subunit-specific recruitment of functional AMPA receptors at neurexin/neuroligin contacts. Proc. Natl. Acad. Sci. USA 105, 20947–20952. 10.1073/pnas.0804007106. [PubMed: 19098102]
25. Fell B, Eckrich S, Blum K, Eckrich T, Hecker D, Obermair GJ, Münkner S, Flockerzi V, Schick B, and Engel J (2016). alpha2delta2 Controls the Function and Trans-Synaptic Coupling of Cav1.3 Channels in Mouse Inner Hair Cells and Is Essential for Normal Hearing. J. Neurosci. 36, 11024–11036. 10.1523/JNEUROSCI.3468-14.2016. [PubMed: 27798183]
26. White JG, Southgate E, Thomson JN, and Brenner S (1986). The structure of the nervous system of *Caenorhabditis elegans*. Phil. Trans. Roy. Soc. Lond. 314, 1–340. [PubMed: 22462104]
27. Liu H, Li L, Wang W, Gong J, Yang X, and Hu Z (2018). Spontaneous Vesicle Fusion Is Differentially Regulated at Cholinergic and GABAergic Synapses. Cell Rep. 22, 2334–2345. 10.1016/j.celrep.2018.02.023. [PubMed: 29490270]
28. Bamber BA, Beg AA, Twyman RE, and Jorgensen EM (1999). The Caenorhabditis elegans unc-49 locus encodes multiple subunits of a heteromultimeric GABA receptor [In Process Citation]. J. Neurosci. 19, 5348–5359. [PubMed: 10377345]
29. Liu P, Ge Q, Chen B, Salkoff L, Kotlikoff MI, and Wang ZW (2011). Genetic dissection of ion currents underlying all-or-none action potentials in C. elegans body-wall muscle cells. J. Physiol. 589, 101–117. 10.1113/jphysiol.2010.200683. [PubMed: 21059759]
30. Lainé V, Frøkjær-Jensen C, Couchoux H, and Jospin M (2011). The alpha1 subunit EGL-19, the alpha2/delta subunit UNC-36, and the beta subunit CCB-1 underlie voltage-dependent calcium currents in Caenorhabditis elegans striated muscle. J. Biol. Chem. 286, 36180–36187. 10.1074/jbc.M111.256149. [PubMed: 21878625]
31. Mueller BD, Merrill SA, Watanabe S, Liu P, Niu L, Singh A, Maldonado-Catala P, Cherry A, Rich MS, Silva M, et al. (2023). CaV1 and CaV2 calcium channels mediate the release of distinct pools of synaptic vesicles. Elife 12, e81407. 10.7554/eLife.81407. [PubMed: 36820519]
32. Bargmann CI (1998). Neurobiology of the Caenorhabditis elegans genome [In Process Citation]. Science 282, 2028–2033. [PubMed: 9851919]

33. Chen RHC, Li Q, Snidal CA, Gardezi SR, and Stanley EF (2017). The Calcium Channel C-Terminal and Synaptic Vesicle Tethering: Analysis by Immuno-Nanogold Localization. Front. Cell. Neurosci. 11, 85. 10.3389/fncel.2017.00085. [PubMed: 28424589]
34. Nieto-Rostro M, Ramgoolam K, Pratt WS, Kulik A, and Dolphin AC (2018). Ablation of alpha(2)delta-1 inhibits cell-surface trafficking of endogenous N-type calcium channels in the pain pathway in vivo. Proc. Natl. Acad. Sci. USA 115, E12043–E12052. 10.1073/pnas.1811212115. [PubMed: 30487217]
35. Tong XJ, Hu Z, Liu Y, Anderson D, and Kaplan JM (2015). A network of autism linked genes stabilizes two pools of synaptic GABA(A) receptors. Elife 4, e09648. 10.7554/eLife.09648. [PubMed: 26575289]
36. Tu H, Pinan-Lucarre B, Ji T, Jospin M, and Bessereau JL (2015). C. elegans Punctin Clusters GABA Receptors via Neuroligin Binding and UNC-40/DCC Recruitment. Neuron. 10.1016/j.neuron.2015.05.013.
37. Maro GS, Gao S, Olechwier AM, Hung WL, Liu M, Özkan E, Zhen M, and Shen K (2015). MADD-4/Punctin and Neurexin Organize C. elegans GABAergic Postsynapses through Neuroligin. Neuron 86, 1420–1432. 10.1016/j.neuron.2015.05.015. [PubMed: 26028574]
38. Zhou X, Gueydan M, Jospin M, Ji T, Valfort A, Pinan-Lucarré B, and Bessereau JL (2020). The netrin receptor UNC-40/DCC assembles a postsynaptic scaffold and sets the synaptic content of GABAA receptors. Nat. Commun. 11, 2674. 10.1038/s41467-020-16473-5. [PubMed: 32471987]
39. Li L, Liu H, Qian KY, Nurrish S, Zeng XT, Zeng WX, Wang J, Kaplan JM, Tong XJ, and Hu Z (2022). CASK and FARP localize two classes of post-synaptic ACh receptors thereby promoting cholinergic transmission. PLoS Genet. 18, e1010211. 10.1371/journal.pgen.1010211. [PubMed: 36279278]
40. Geisler S, Schöpf CL, Stanika R, Kalb M, Campiglio M, Repetto D, Traxler L, Missler M, and Obermair GJ (2019). Presynaptic alpha2delta-2 Calcium Channel Subunits Regulate Postsynaptic GABAA Receptor Abundance and Axonal Wiring. J. Neurosci. 39, 2581–2605. 10.1523/JNEUROSCI.2234-18.2019. [PubMed: 30683685]
41. Crosby KC, Gookin SE, Garcia JD, Hahm KM, Dell'Acqua ML, and Smith KR (2019). Nanoscale Subsynaptic Domains Underlie the Organization of the Inhibitory Synapse. Cell Rep. 26, 3284–3297.e3. 10.1016/j.celrep.2019.02.070. [PubMed: 30893601]
42. Schopf CL, Ablinger C, Geisler SM, Stanika RI, Campiglio M, Kaufmann WA, Nimmervoll B, Schlick B, Brockhaus J, Missler M, et al. (2021). Presynaptic alpha2delta subunits are key organizers of glutamatergic synapses. Proc. Natl. Acad. Sci. USA 118. 10.1073/pnas.1920827118.
43. Tracy TE, Yan JJ, and Chen L (2011). Acute knockdown of AMPA receptors reveals a trans-synaptic signal for presynaptic maturation. EMBO J. 30, 1577–1592. 10.1038/emboj.2011.59. [PubMed: 21378752]
44. Orr BO, Hauswirth AG, Celona B, Fetter RD, Zunino G, Kvon EZ, Zhu Y, Pennacchio LA, Black BL, and Davis GW (2020). Presynaptic Homeostasis Opposes Disease Progression in Mouse Models of ALS-Like Degeneration: Evidence for Homeostatic Neuroprotection. Neuron 107, 95–111.e6. 10.1016/j.neuron.2020.04.009. [PubMed: 32380032]
45. Delvendahl I, and Müller M (2019). Homeostatic plasticity-a presynaptic perspective. Curr. Opin. Neurobiol. 54, 155–162. 10.1016/j.conb.2018.10.003. [PubMed: 30384022]
46. Meyer D, Bonhoeffer T, and Scheuss V (2014). Balance and stability of synaptic structures during synaptic plasticity. Neuron 82, 430–443. 10.1016/j.neuron.2014.02.031. [PubMed: 24742464]
47. Schikorski T, and Stevens CF (1997). Quantitative ultrastructural analysis of hippocampal excitatory synapses. J. Neurosci. 17, 5858–5867. [PubMed: 9221783]
48. Lisman JE, and Harris KM (1993). Quantal analysis and synaptic anatomy–integrating two views of hippocampal plasticity. Trends Neurosci. 16, 141–147. 10.1016/0166-2236(93)90122-3. [PubMed: 7682347]
49. Dittman JS, and Kaplan JM (2006). Factors regulating the abundance and localization of synaptobrevin in the plasma membrane. Proc. Natl. Acad. Sci. USA 103, 11399–11404. [PubMed: 16844789]

50. Frøkjaer-Jensen C, Davis MW, Hopkins CE, Newman BJ, Thummel JM, Olesen SP, Grunnet M, and Jorgensen EM (2008). Single-copy insertion of transgenes in Caenorhabditis elegans. Nat. Genet. 40, 1375–1383. 10.1038/ng.248. [PubMed: 18953339]

51. Frøkjær-Jensen C, Davis MW, Sarov M, Taylor J, Flibotte S, LaBella M, Pozniakovsky A, Moerman DG, and Jorgensen EM (2014). Random and targeted transgene insertion in Caenorhabditis elegans using a modified Mos1 transposon. Nat. Methods 11, 529–534. 10.1038/nmeth.2889. [PubMed: 24820376]

52. Arribere JA, Bell RT, Fu BXH, Artiles KL, Hartman PS, and Fire AZ (2014). Efficient marker-free recovery of custom genetic modifications with CRISPR/Cas9 in Caenorhabditis elegans. Genetics 198, 837–846. 10.1534/genetics.114.169730. [PubMed: 25161212]

53. Feng S, Sekine S, Pessino V, Li H, Leonetti MD, and Huang B (2017). Improved split fluorescent proteins for endogenous protein labeling. Nat. Commun. 8, 370. 10.1038/s41467-017-00494-8. [PubMed: 28851864]

54. Schnütgen F, and Ghyselinck NB (2007). Adopting the good reFLEXes when generating conditional alterations in the mouse genome. Transgenic Res. 16, 405–413. 10.1007/s11248-007-9089-8. [PubMed: 17415672]

- Muscle $GABA_A$ receptors boost GABA release by recruiting CaV2 to active zones
- Clustered post-synaptic $GABA_A$ receptors mediate retrograde synaptic potentiation
- Extra-synaptic $GABA_A$ receptors have no retrograde effects
- The *C. elegans* GABAergic NMJ does not exhibit pre-synaptic homeostatic plasticity

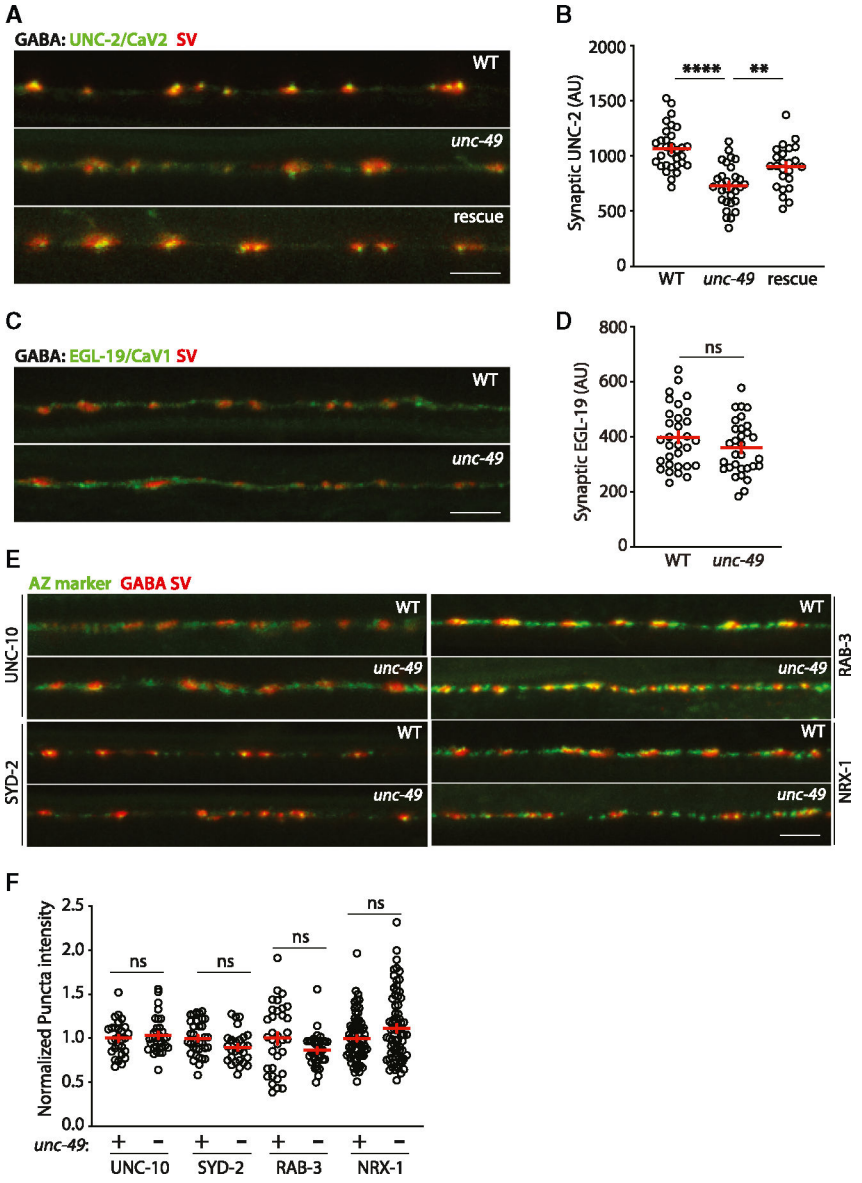

Figure 1. UNC-2/CaV2 levels at GABA neuron active zones are decreased in mutants lacking UNC-49/GABA$_A$ receptors

(A–D) Pre-synaptic abundance of GFP$_{11}$-tagged UNC-2/CaV1 (A and B) and EGL-19/CaV1 (C and D) was analyzed in GABA motor neurons. CRISPR alleles were constructed adding seven copies of GFP$_{11}$ to the endogenous *egl-19* and *unc-2* genes (key resources table), fluorescence was reconstituted by expressing GFP$_{1–10}$ in GABA neurons, and pre-synaptic terminals were identified by expressing mCherry-tagged UNC-57/endophilin (which associates with synaptic vesicles). Controls showing that the GFP$_{11}$ tags had no effect on EGL-19 and UNC-2 function are shown in Figure S1. Representative images (A and C) and mean intensity of pre-synaptic CaV puncta (B and D) in dorsal cord axons are shown. UNC-2 puncta intensity was significantly decreased in *unc-49* GABA$_A$ mutants, and this defect was rescued by a transgene expressing UNC-49B in muscles. By contrast, EGL-19 puncta intensity was unaffected in *unc-49* GABA$_A$ mutants.

(E and F) Other AZ markers were unaffected in *unc-49* $GABA_A$ mutants. The abundance of several AZ proteins (UNC-10/RIM, SYD-2/liprin-α, RAB-3, and NRX-1/neurexin-α) was quantified in GABA neuron dorsal cord axons. Each AZ protein was visualized using CRISPR alleles containing fluorescent protein tags in the corresponding endogenous gene. GABA and ACh neuron puncta were distinguished by expressing mCherry-tagged UNC-57/endophilin in GABA neurons. (E) Representative images of AZ proteins at GABA pre-synapses (defined by the UNC-57 signal) in dorsal cord axons are compared in WT and *unc-49* mutants. (F) Mean GABA neuron AZ puncta intensity is plotted (normalized to the mean WT value for each protein). No significant differences were observed. Sample sizes: (B) WT (31), *unc-49* (31), and rescue (24); (D) WT (31) and *unc-49* (31); (F) *unc-10*(wy1417) (28), *unc-49;unc-10*(wy1417) (33), *syd-2*(wy1052) (34), *syd-2(wy1052);unc-49* (27), *rab-3(wy1419)* (34), *rab-3(wy1419);unc-49* (36), *nrx-1(nu742)* (71), and *nrx-1(nu742);unc-49* (73). Values that differ significantly from wild-type controls are indicated (ns, not significant; $^{**}p < 0.01$; $^{***}p < 0.001$). Statistical tests: ordinary one way ANOVA with Tukey's multiple comparisons test (B); unpaired t test (D); Kruskal-Wallis test with Dunn's multiple comparisons test (F). Error bars: SEM. Scale bars: 5 μm.

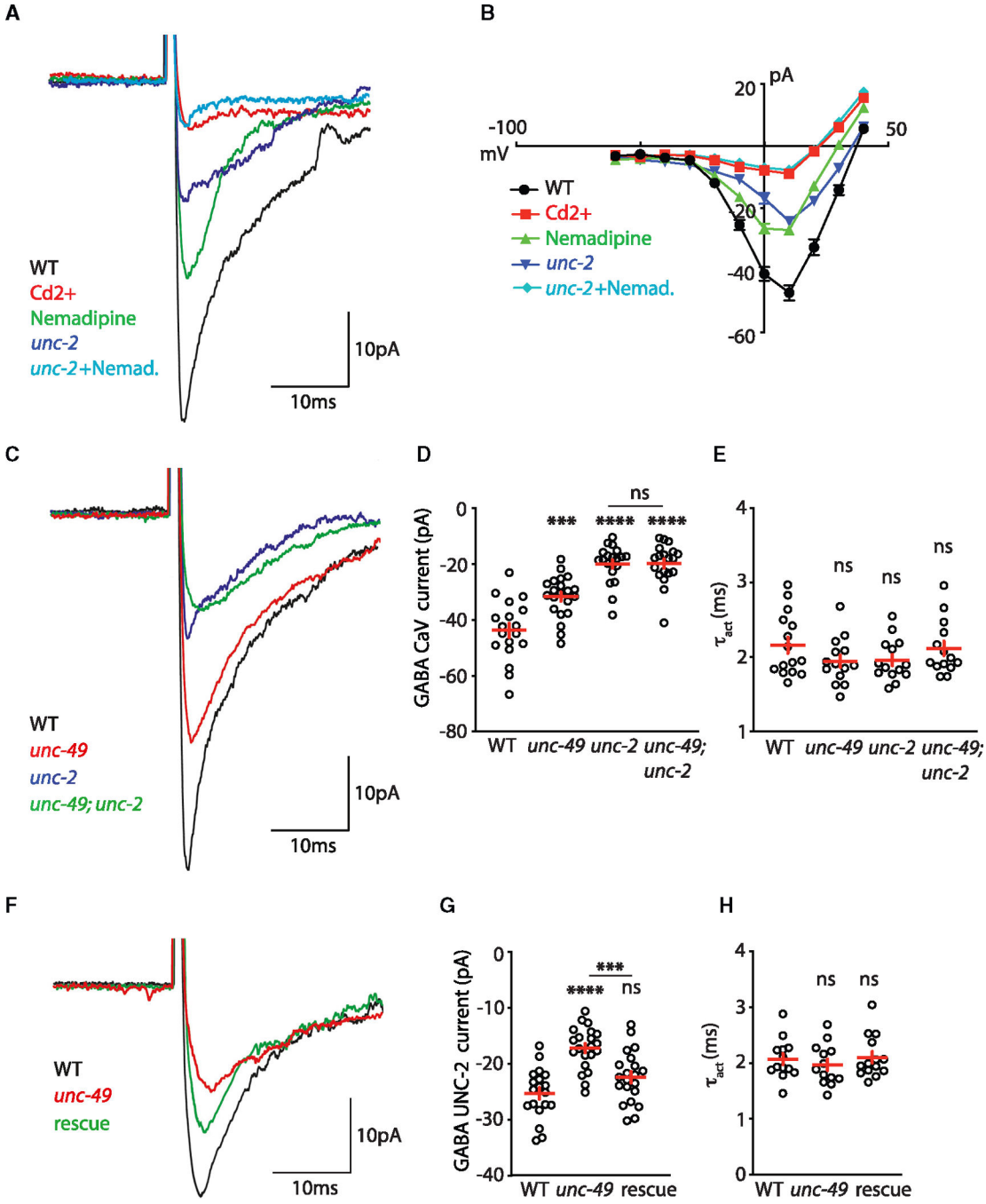

Figure 2. UNC-2/CaV2 currents in GABA motor neuron are decreased in mutants lacking UNC-49/GABA$_A$ receptors

(A and B) Voltage-activated calcium currents (I_{CaV}) were recorded from GABA motor neurons in the ventral nerve cord. Representative traces (at 0 mV), and mean I_{CaV} current as a function of membrane potential are shown. I_{CaV} was eliminated by a general CaV pore blocker (Cd^{2+}), was reduced 50% by an EGL-19 CaV1 antagonist (nemadipine) and in *unc-2* CaV2 mutants, and was eliminated in nemadipine-treated *unc-2* CaV2 mutants. (C–H) I_{CaV} was significantly decreased in *unc-49* GABA$_A$ mutants. Total I_{CaV} current (C and E) and UNC-2 current isolated by nemadipine treatment (F–H) were recorded

from GABA motor neurons (at 0 mV). Representative traces (C and F), mean current amplitude (D and G), and mean current activation time constant (E and H) are shown. The I_{CaV} defect in *unc-49* mutants was eliminated in double mutants lacking *unc-2* CaV2 (C and D), was unaffected by nemadipine treatment (F and G), and was rescued by a transgene restoring UNC-49B expression in muscles (F and G). Sample sizes: (D) WT (18), *unc-49* (21), *unc-2* (20), and *unc-49;unc-2* (19); (E) WT (15), *unc-49* (14), *unc-2* (14), and *unc-49;unc-2* (14); (G) WT (19), *unc-49* (21), and rescue (21); (H) WT (13), *unc-49* (13), and rescue (14). Values that differ significantly from wild-type controls are indicated (ns, not significant; ***$p < 0.001$; ****$p < 0.0001$). Statistical tests: ordinary one way ANOVA with Tukey's multiple comparisons test (D, E, and G); Kruskal-Wallis test with Dunn's multiple comparisons test (H). Error bars: SEM.

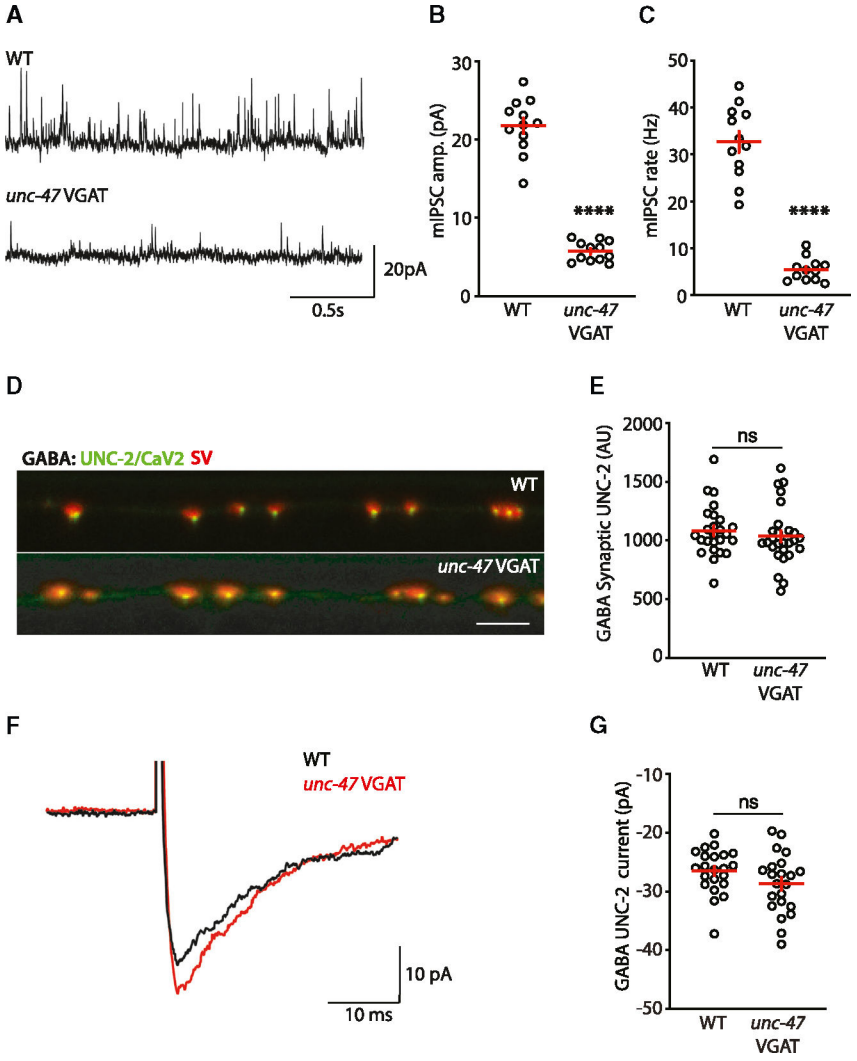

Figure 3. Blocking GABA release has no effect on GABA neuron UNC-2/CaV2 levels

(A–C) Controls documenting GABA release defects in *unc-47* VGAT mutants are shown. Spontaneous miniature inhibitory post-synaptic currents (mIPSCs) were recorded from body muscles. Representative traces (A), mean mIPSC amplitude (B), and mean mIPSC rate (C) are shown.

(D and E) UNC-2/CaV2(GFP_{11}) puncta intensity in dorsal cord GABA axons are compared in WT and *unc-47* VGAT mutants. Representative images (D) and mean UNC-2 puncta intensity (E) are shown. (F and G) UNC-2/CaV2 current recorded from GABA motor neurons (at 0 mV) is compared in WT and *unc-47* VGAT mutants. Representative traces (F) and mean current amplitude (G) are shown. Sample sizes: (B and C) WT (12) and *unc-47* (12); (E) WT (25) and *unc-47* (27); (G) WT (22) and *unc-47* (22). Values that differ significantly from wild-type controls are indicated (ns, not significant; ****$p < 0.0001$). Statistical tests: unpaired t test (B, C, and G); Mann-Whitney test (E). Error bars: SEM. Scale bar: 5 μm.

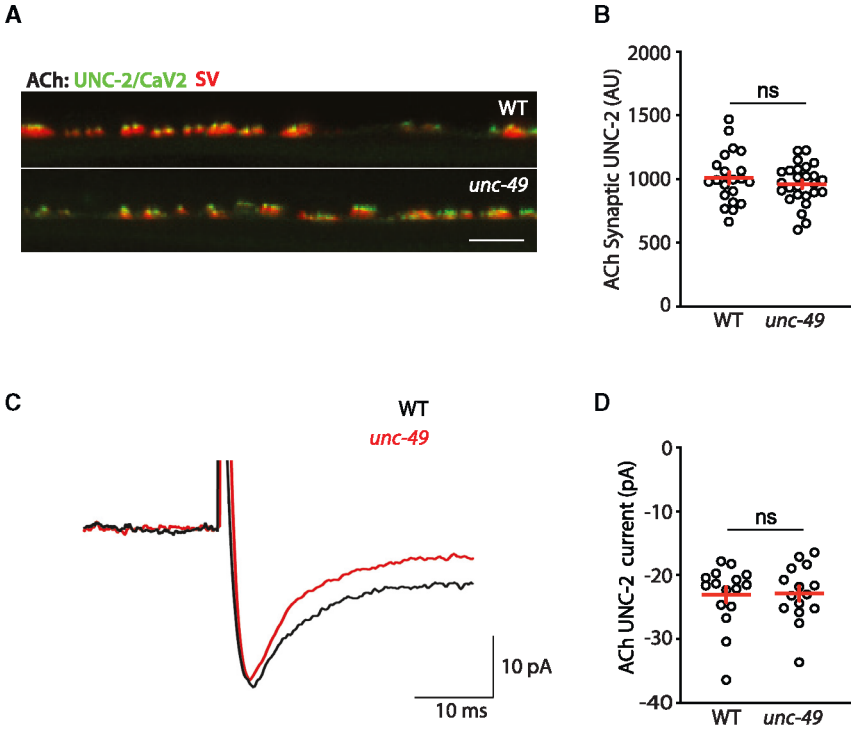

Figure 4. ACh motor neuron UNC-2/CaV2 levels were unaltered in *unc-49* $GABA_A$ mutants

(A and B) UNC-2/CaV2(GFP_{11}) puncta intensity in dorsal cord ACh neuron axons is compared in WT and *unc-49* $GABA_A$ mutants. Representative images (A) and mean UNC-2 puncta intensity (B) are shown. (C and D) UNC-2/CaV2 current recorded from ACh motor neurons (at 0 mV) is compared in WT and *unc-49* $GABA_A$ mutants. Representative traces (C) and mean current amplitude (D) are shown. Sample sizes: (B) WT (21) and unc-49 (26); (D) WT (16) and *unc-49* (15). No significant differences were observed: unpaired t test (B), Mann-Whitney (D). Error bars: SEM. Scale bar: 5 μm.

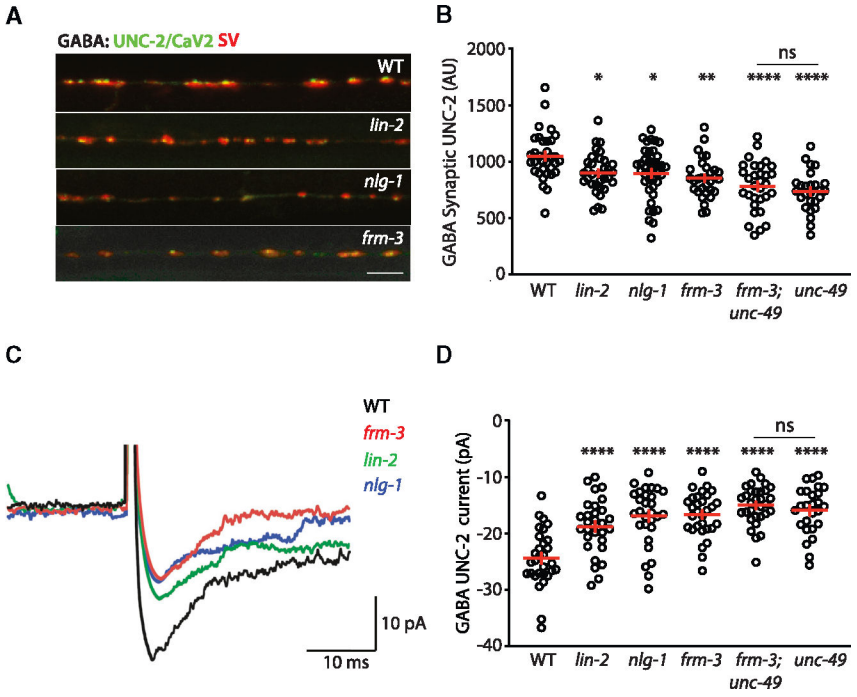

Figure 5. Clustered synaptic UNC-49/GABA$_A$ receptors are required for UNC-2/CaV2 localization in GABA axons

(A and B) UNC-2/CaV2(GFP$_{11}$) puncta intensity in dorsal cord GABA axons is compared in WT and mutants lacking scaffold proteins (FRM-3/FARP, LIN-2/CASK, and NLG-1/neuroligin) that localize UNC-49 to post-synapses. Representative images (A) and mean UNC-2 puncta intensity (B) are shown. (C and D) UNC-2/CaV2 current recorded from GABA motor neurons (at 0 mV) is compared in WT and scaffold mutants. Representative traces (C) and mean current amplitude (D) are shown. UNC-2/CaV2 puncta intensity and current were significantly reduced in all scaffold single mutants. The synaptic UNC-2 levels and current observed in *unc-49* single mutants were not further reduced in *frm-3;unc-49* double mutants, indicating that FRM-3 and UNC-49 act together to regulate UNC-2. Sample sizes: (B) WT (33), *lin-2* (33), *nlg-1* (39), *frm-3* (32), *frm-3;unc-49* (31), and *unc-49* (26); (D) WT (30), *lin-2* (29), *nlg-1* (29), *frm-3* (30), *frm-3;unc-49* (31), and *unc-49* (26). Values that differ significantly from wild-type controls are indicated (ordinary one way ANOVA with Tukey's multiple comparisons test; ns, not significant; *p < 0.05; **p < 0.01; ****p < 0.0001). Error bars: SEM. Scale bar: 5 μm.

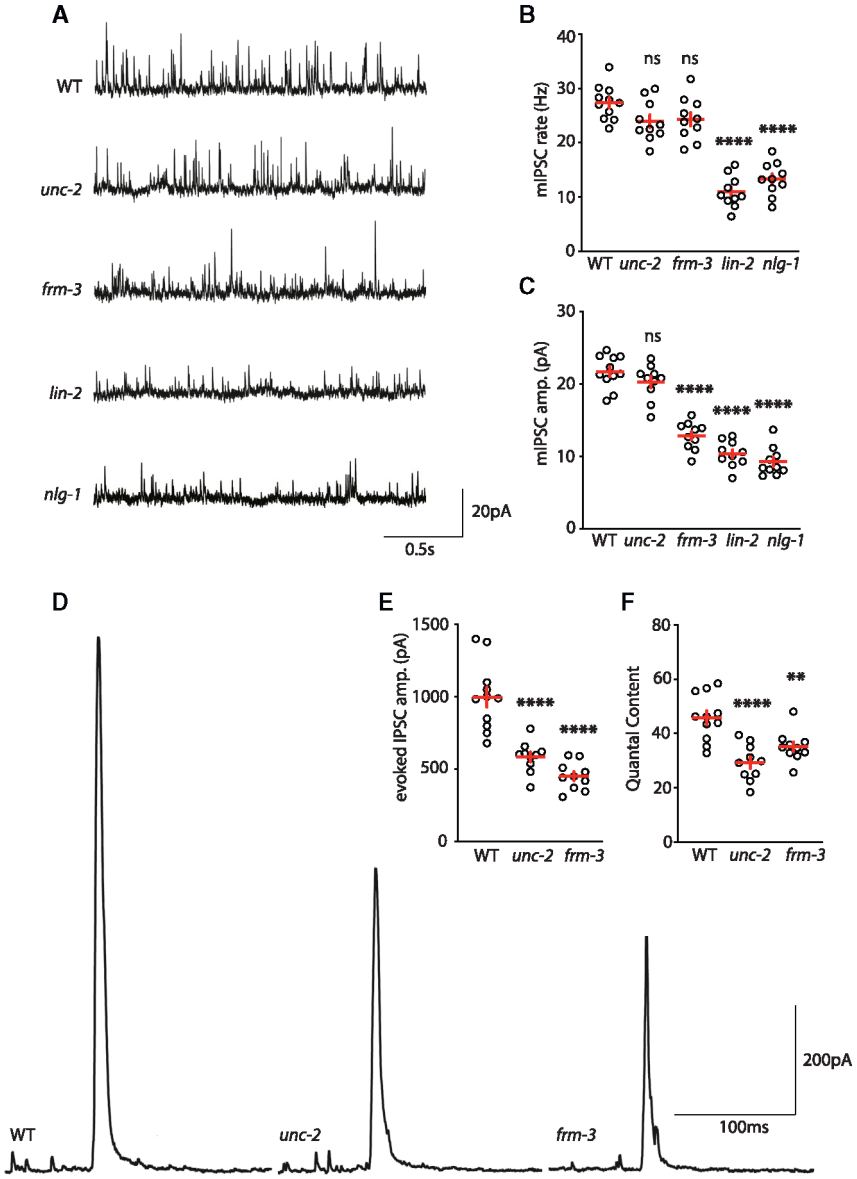

Figure 6. GABA release at NMJs is decreased in *frm-3* FARP mutants

GABA release at NMJs was assessed by recording muscle inhibitory post-synaptic currents (IPSCs). (A–C) Spontaneous miniature IPSCs (mIPSCs) were recorded in the indicated genotypes. Representative traces (A), mean mIPSC amplitude (B), and mean mIPSC rate (C) are shown. As previously reported, mIPSC amplitudes were significantly reduced in mutants lacking synaptic scaffolding proteins (FRM-3, LIN-2, and NLG-1) due to the reduced clustering of UNC-49 receptors at post-synapses in these mutants.[35–38] The mIPSC rate was also reduced in *lin-2* and *nlg-1*, most likely due to decreased detection of the smaller mIPSCs. By contrast, mIPSC rate was unaffected in *frm-3* mutants, perhaps due to the somewhat smaller decrease in mIPSC amplitudes in these mutants. mIPSC amplitude and rate were unaffected in *unc-2* CaV2 null mutants.

(D and F) Evoked IPSCs were recorded following optogenetic activation of GABA motor neurons. Representative traces (D), evoked IPSC amplitude (E), and quantal content (QC)

of evoked responses (F) are shown. QC is a measure of the total number of SVs released during an evoked IPSC. QC was calculated as the ratio of the amplitude in evoked IPSCs to the mean mIPSC amplitude in the same animal. QC was significantly decreased in *frm-3* and *unc-2* mutants, indicating decreased GABA release. Sample sizes: (B and C) WT (11), *unc-2* (10), *frm-3* (10), *lin-2* (10), and *nlg-1* (10); (E and F) WT (11), *unc-2* (10), and *frm-3* (10). Values that differ significantly from WT are indicated (ordinary one way ANOVA with Tukey's multiple comparisons test; ns, not significant; **p < 0.01; ****p < 0.0001). Error bars: SEM.

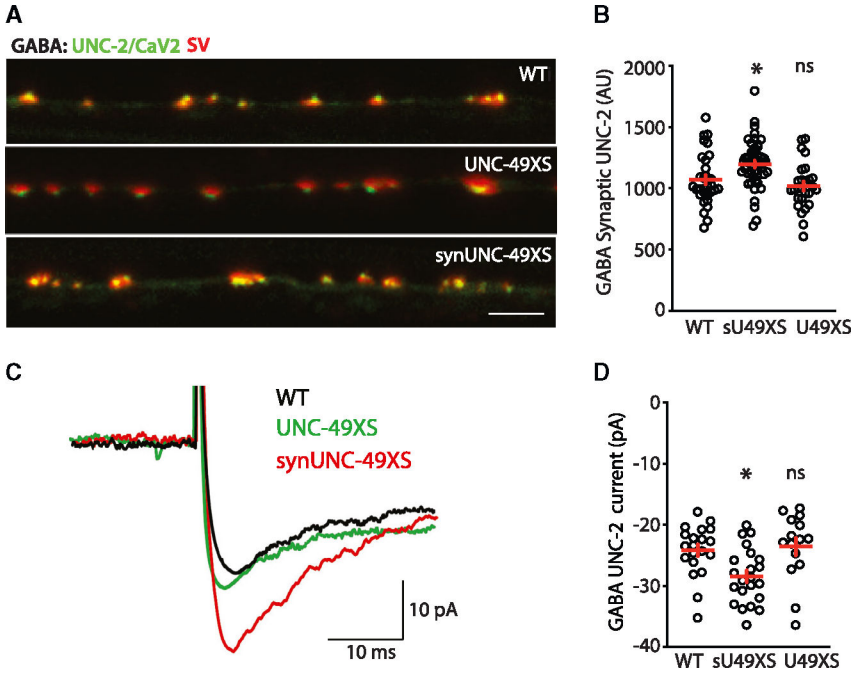

Figure 7. Increasing post-synaptic $GABA_A$ levels produces corresponding increases in GABA neuron CaV2 levels

GABA neuron UNC-2/CaV2 levels and current were analyzed in UNC-49XS and synUNC-49XS animals. (A and B) UNC-2/CaV2(GFP_{11}) puncta intensity in dorsal cord GABA axons are compared in the indicated strains. Representative images (A) and mean UNC-2 puncta intensity (B) are shown.

(C and D) UNC-2/CaV2 current was recorded from GABA motor neurons (at 0 mV). Representative traces (C) and mean current amplitude (D) are shown. UNC-2/CaV2 puncta intensity and current were both significantly increased in synUNC-49XS animals but were unaffected in UNC-49XS animals. These results suggest that CaV2 levels at active zones are increased when post-synaptic $GABA_A$ receptors are increased but are unaffected by increased extra-synaptic receptors. Sample sizes: (B) WT (32), synUNC-49XS (47), and UNC-49XS (27); (D) WT (20), synUNC-49XS (22), and UNC-49XS (15). Values that differ significantly from WT are indicated (ordinary one way ANOVA with Tukey's multiple comparisons test; ns, not significant; *$p < 0.05$). Error bars: SEM. Scale bar: 5 μm.

KEY RESOURCES TABLE

REAGENT or RESOURCE	SOURCE	IDENTIFIER
Chemicals, peptides, and recombinant proteins		
Nemadipine-A L-type calcium channel protein inhibitor	ABCAM	Catalog #:ab145991
Experimental models: Organisms/strains		
strain (*C. elegans*) N2	CGC	Wormbase ID:N2
C. elegans: Strain KP10679 frm- 3(nu751) ON; unc-2(nu586); nuSi285 nu751 is a CRE inactivated allele; nuSi285 is Punc-47:GFP1-10:sl2:unc57mCherry:sl2:mTaqBFP2	This study	KP10679
C. elegans: Strain KP10692 frm- 3(nu751) ON; nuSi572; unc-2(nu586); nuSi285 nuSi572 is Pmyo-3: NLS CRE SL2 NLS BFP	This study	KP10692
strain (*C. elegans*) KP10675 frm- 3(nu751) ON; nuSi502; unc-2(nu586); nuSi285 nuSi502 is Psbt-1: NLS CRE SL2 NLS BFP	This study	KP10675
strain (*C. elegans*) KP10506 nrx-1(nu742) nu742 contains mNG inserted at codon 1515 of NRX-1A	This study	KP10506
strain (*C. elegans*) KP9639 nuSi285; unc-2(nu586) nu586 contains 7 GFP11 copies inserted at codon 2013 of UNC-2B	This study	KP9639
strain (*C. elegans*) KP11018 unc-49(e407); nuSi285; unc-2(nu586)	This study	KP11018
strain (*C. elegans*) KP11021 syd-2(wy1052); nuSi285 wy1052 contains GFP inserted at codon 2 of SYD-2	This study	KP11021
strain (*C. elegans*) KP11022 unc-49(e407); syd-2(wy1052); nuSi285	This study	KP11022
strain (*C. elegans*) KP11023 unc-10(wy1417); nuSi285	This study	KP11023
strain (*C. elegans*) KP11024 unc-49(e407); unc-10(wy1417); nuSi285 wy1417 contains GFP inserted in the last exon of UNC-10	This study	KP11024
strain (*C. elegans*) KP11025 UNC-49XS(nuEx2039) The UNC-49XS(nuEx2039) transgene is Ppat-10: UNC-49B; Punc-122:gfp	This study	KP11025
strain (*C. elegans*) KP11026 rab-3(wy1419); nuSi285 wy1419 contains GFP inserted at codon 2 of RAB-3	This study	KP11026
strain (*C. elegans*) KP11027 unc- 49(e407); rab-3(wy1419); nuSi285	This study	KP11027
strain (*C. elegans*) KP11028 unc-47(gk192); nuSi285; unc-2(nu586)	This study	KP11028
strain (*C. elegans*) KP11029 unc- 47(gk192); nuEx1067 nuEx1067 is the Punc-47:GFP transgene	This study	KP11029
strain (*C. elegans*) KP11030 nuSi285; unc-2(nu586); nuEx1067	This study	KP11030
strain (*C. elegans*) KP11031 nrx- 1(nu742); nuSi285	This study	KP11031
strain (*C. elegans*) KP11032 unc- 49(e407); nrx-1(nu742); nuSi285	This study	KP11032
strain (*C. elegans*) KP11033 nlg- 1(ok259); nuSi285; unc-2(nu586)	This study	KP11033
strain (*C. elegans*) KP11034 nlg-1 (ok259); nuEx1067	This study	KP11034
strain (*C. elegans*) KP11035 lin- 2(syb1019); nuSi285; unc-2(nu586)	This study	KP11035
strain (*C. elegans*) KP11036 lin-2(syb1019); nuEx1067	This study	KP11036
strain (*C. elegans*) KP11037 frm- 3(gk585); nuSi285; unc-2(nu586)	This study	KP11037
strain (*C. elegans*) KP11038 frm- 3(gk585); nuEx1067(nuEx1067)	This study	KP11038
strain (*C. elegans*) KP11039 frm- 3(gk585); unc-49(e407); nuSi285; unc- 2(nu586)	This study	KP11039
strain (*C. elegans*) KP11040 frm- 3(gk585); unc-49(e407); nuEx1067	This study	KP11040

REAGENT or RESOURCE	SOURCE	IDENTIFIER
strain (*C. elegans*) KP11041 synUNC-49XS(nuIs633); nuSi285; unc-2(nu586) synUNC-49XS(nuIs633) expresses UNC-49B, NLG-1F, LIN-2A, and FRM-3A in muscles	This study	KP11041
strain (*C. elegans*) KP11042 synUNC-49XS(nuIs633); nuEx1067 synUNC-49XS(nuIs633) expresses UNC-49B, NLG-1F, LIN-2A, and FRM-3A in muscles	This study	KP11042
strain (*C. elegans*) KP11043 UNC-49XS(nuEx2039); nuSi285; unc-2(nu586) UNC-49XS(nuEx2039) is Ppat-10:UNC-49B; Punc-122:gfp	This study	KP11043
strain (*C. elegans*) KP11044 UNC-49XS(nuEx2039 unc-49b/gfp); nuEx1067 UNC-49XS(nuEx2039) is Ppat-10:UNC-49B; Punc-122:gfp	This study	KP11044
strain (*C. elegans*) PHX1019 lin- 2(syb1019)	Zhitao Hu	PHX1019
strain (*C. elegans*) VC1288 frm- 3(gk585)	CGC	VC1288
strain (*C. elegans*) VC311 unc- 47(gk192)	CGC	VC311
strain (*C. elegans*) VC854 unc- 2(gk366)	CGC	VC854
strain (*C. elegans*) KP10999 synUNC- 49XS(nuIs633) synUNC-49XS(nuIs633) expresses UNC-49B, NLG-1F, LIN-2A, and FRM-3A in muscles	This study	KP10999
strain (*C. elegans*) KP11046 egl- 19(nu674); nuSi285 nu674 contains 7 GFP11 copies inserted at codon 2 of EGL-19	This study	KP11046
strain (*C. elegans*) KP9809 unc- 2(nu586); nuSi250 nuSi250 is Punc-129 GFP 1-10 SL2 unc-57:mCherry SL2 BFP	This study	KP9809
strain (*C. elegans*) KP11047 unc- 49(e407); unc-2(nu586); nuSi250	This study	KP11047
strain (*C. elegans*) KP11054 unc- 49(e407); synUNC-49XS(nuSi633)	This study	KP11054
strain (*C. elegans*) KP11049 unc- 49(e407); vsIs48 vsIs48 is the Punc-17:GFP transgene	This study	KP11049
strain (*C. elegans*) KP11051 unc- 49(e407); synUNC-49XS(nuSi633); nuSi285; unc- 2(nu586)	This study	KP11051
strain (*C. elegans*) KP11052 unc- 49(e407); synUNC-49XS(nuSi633); nuEx1067	This study	KP11052
strain (*C. elegans*) KP11053 unc- 49(e407))egl-19(nu674); nuSi285	This study	KP11053
strain (*C. elegans*) KP11048 UNC- 49(e407); nuEx1067	This study	KP11048
strain (*C. elegans*) KP11056 unc- 49(e407); unc-2(gk366); nuEx1067	This study	KP11056
strain (*C. elegans*) LX929 vsIs48 [unc-17:GFP]	CGC	LX929
strain (*C. elegans*) ZX426 zxIs3[Punc- 47:ChR2(H134R): YFP; lin-15+]I	Alexander Gottschalk	ZX426
strain (*C. elegans*) KP11057 lin- 2(syb1019); zxIs3	This study	KP11057
strain (*C. elegans*) KP11058 frm- 3(gk585); zxIs3	This study	KP11058
strain (*C. elegans*) KP11059 unc- 2(gk366); zxIs3	This study	KP11059
strain (*C. elegans*) KP11060 nlg-1 (ok259); zxIs3	This study	KP11060
strain (*C. elegans*) KP11061 unc- 2(gk366); nuEx1067	This study	KP11061
strain (*C. elegans*) KP11062 frm- 3(nu751) ON; unc- 2(nu586); nuSi285; nuEx1067	This study	KP11062
strain (*C. elegans*) KP11063 frm- 3(nu751) ON; nuSi572; unc-2(nu586); nuSi285; nuEx1067 nuSi572 is Pmyo-3: NLS CRE SL2 NLS BFP	This study	KP11063
strain (*C. elegans*) KP11064 frm- 3(nu751) ON; nuSi502; unc-2(nu586); nuSi285; nuEx1067 nuSi502 is Psbt-1: NLS CRE SL2 NLS BFP	This study	KP11064

REAGENT or RESOURCE	SOURCE	IDENTIFIER
strain (*C. elegans*) VC228 nlg- 1(ok259) X	CGC	VC228
strain (*C. elegans*) KP11174 unc- 2(nu657 mNG FLEX); nuSi285 nu657 contains mNG inserted at codon 2013 of UNC-2B and an inverted terminator cassette in intron 15	This study	KP11174
strain (*C. elegans*) KP11175 unc- 49(e407); unc-2(nu657 mNG FLEX); nuSi285	This study	KP11175
Oligonucleotides		
gctattaccgcgcctttcagCGG	IDT	guide RNA for nrx-1 neonGreen insertion
tacacacatgcacacgtcggGGG	IDT	guide RNA for FLEX insertion into the 3rd intron of frm-3
tctgtttccgagtcagatagTGG	IDT	guide RNA for x7 GFP11 insertion at unc-2 codon 2013
ttacctgacatgatggacacAGG	IDT	guide RNA for x7 GFP11 insertion at egl-19 codon 2
Recombinant DNA		
Plasmid: KP#4527 Pmyo-3 NLS CRE miniMOS hyg	This study	Expresses nuclear localized CRE recombinase in body wall muscles
Plasmid: KP#4528 Psbt-1 NLS CRE SL2A NLS BFP miniMOS hyg	This study	Expresses nuclear localized CRE recombinase and BFP in neurons
Plasmid: KP#4532 Ppat-10 unc-49B cDNA miniMOS hyg	This study	Expresses UNC-49B cDNA in body wall muscles
Plasmid: KP#1786 Pmyo-3 NLG-1F cDNA	This study	Expresses NLG-1F cDNA in body wall muscles
Plasmid: KP#1795 Pmyo-3 LIN-2A cDNA	This study	Expresses LIN-2A cDNA in body wall muscles
Plasmid: KP#2220 Pmyo-3 FRM-3A cDNA	This study	Expresses FRM-3A cDNA in body wall muscles
Plasmid: KP#4532 Punc-47:gfp1-10 SL2 unc-57:mCherry	This study	Expresses sfGFP1-10 and UNC-57: mCherry in GABAergic cells
Plasmid: KP#4525 Punc-129:gfp1-10 SL2 unc-57:mCherry	This study	Expresses sfGFP1-10 and UNC-57: mCherry in DA and DB motorneurons
Software and algorithms		
ImageJ/Fiji	NIH	https://fiji.sc/
pClamp 10	Molecular Devices	https://www.moleculardevices.com
Prism9	GraphPad	https://www.graphpad.com
OriginLab	OriginLab	https://www.originlab.com/
NIS Elements	Nikon	https://www.microscope.healthcare.nikon.com/
Other		
Polybead Microspheres 0.10μm	POLYSCIENCES INC	Catalog#: 00876-15